Metabolic regulation of differentiation and maturation: from induced pluripotent stem cell to endothelial cell

Es - Tiemeier, G.L. van

Chapter 3

Lowering the Increased Intracellular pH of Human iPSC-Derived Endothelial Cells Induces Formation of Mature Weibel Palade Bodies.

Gesa L. Tiemeier[1], Rozemarijn de Koning[1], Gangqi Wang[1], Sarantos Kostidis[2], Rosalie G.J. Rietjens[1], Wendy M.P.J. Sol[1], Sébastien J. Dumas[3,4], Martin Giera[2], Cathelijne W. van den Berg[1], Jeroen C.J. Eikenboom[5], Bernard van den Berg[1], Peter Carmeliet[3,4], Ton J. Rabelink[1]

[1] The Einthoven Laboratory for Vascular and Regenerative Medicine, Department of Internal Medicine, Division of Nephrology, Leiden University Medical Center, Leiden, The Netherlands.
[2] Center for Proteomics & Metabolomics, Leiden University Medical Center, Leiden, the Netherlands.
[3] Laboratory of Angiogenesis and Vascular Metabolism, Department of Oncology, KU Leuven, Leuven, Belgium.
[4] Laboratory of Angiogenesis and Vascular Metabolism, Center for Cancer Biology, VIB, Leuven, Belgium.
[5] Department of Thrombosis and Hemostasis, Einthoven Laboratory for Experimental Vascular Medicine, Leiden University Medical Center, Leiden, The Netherlands

Stem Cells Translational Medicine - 2020 Jul;9(7):758-772.

Abstract

Differentiation of human induced pluripotent stem cells (hiPSCs) into vascular endothelium is of great importance to tissue engineering, disease modelling and use in regenerative medicine. Although differentiation of hiPSCs into endothelial-like cells (hiPSC-ECs) has been demonstrated before, controversy exists as to what extend these cells faithfully reflect mature endothelium. To address this issue, we investigate hiPSC-ECs maturation by their ability to express von Willebrand Factor (VWF) and formation of Weibel Palade Bodies (WPBs). Using multiple hiPSCs lines, hiPSC-ECs failed to form proper VWF and WPBs, essential for angiogenesis, primary and secondary homeostasis. Lowering the increased intracellular pH (pHi) of hiPSC-ECs with acetic acid did result in the formation of elongated WPBs. NMR data showed that the higher pHi in hiPSC-ECs occurred in association with decreased intracellular lactate concentrations. This was explained by decreased glycolytic flux towards pyruvate and lactate in hiPSC-ECs. In addition, decreased expression of MCT1, a member of the solute carrier family (SLC16A1) which regulates lactate and H+ uptake, contributed to the high pHi of hiPSC-EC. Mechanistically, pro-VWF dimers require the lower pH environment of the trans-Golgi network (TGN) for maturation and tubulation. These data show, that while hiPSC-ECs may share many features with mature EC, they are characterised by metabolic immaturity hampering proper EC function.

Introduction

Recent developments in stem cell biology have enabled differentiation of reprogrammed cells into the cell type of interest, a phenomenon that opened up many opportunities for studying organogenesis and repair, disease modeling with organoids and patient specific cell therapy. A functional vasculature, however, is a prerequisite to realize these opportunities and differentiation of human induced pluripotent stem cells (hiPSC) into proper functioning endothelium will be key to unlock the potential of reprogramming-based strategies [1-7]. Recent studies characterized hiPSC-derived endothelial cells (hiPSC-ECs) and concluded that although hiPSC-ECs demonstrate a spectrum of physiological endothelial functions, the punctate perinuclear localization of von Willebrand Factor (VWF) may suggest an immature stage of Weibel Palade Bodies (WPBs) biogenesis [8,9].

Endothelial cells (ECs) are key regulators of vascular haemostasis by producing VWF, a multimeric glycoprotein[10-12]. After excretion at the site of vascular injury, VWF chaperones and protects blood coagulation factor VIII from proteolytic inactivation and binds to glycoprotein Ib (GPIb) receptors on platelets, as well as collagen and heparin, and is therefore involved in both primary and secondary haemostasis [11,13].

Biosynthesis of VWF emerges in the endoplasmic reticulum (ER), where VWF precursor proteins consisting of a signal peptide, N-terminal propeptide and a mature peptide start to dimerize through the C-terminal cysteine knot (CK) domain interactions. Subsequently, disulphide bonding between D'-D3 domains initiate multimerization in the Golgi [14-17]. The final processing of VWF takes place at the *trans*-Golgi network (TGN) where pro-VWF is cleaved by furin and VWF is either stored in endothelial specific elongated cigar-shaped secretory organelles named Weibel Palade Bodies (WPBs) or constitutively secreted [14,18-20] Prior to WPB storage, highly multimerized VWF proteins start to form tubules, which create the striated appearance of WPBs. WPB formation is driven by the presence of VWF protein as introduction of VWF in non-ECs has shown to stimulate formation of WPB-like storage organelles [18,21,22]. Tubulation allows a 100-fold compaction of VWF and drives the formation of elongated WPBs, which is achieved through low-pH dependent interactions between the VWF propeptide and N-terminal region of mature VWF [20,23]. Furthermore, tubulation is necessary for the rapid unfurling of ultralong VWF filaments, caused by the shift from the acidic WPB (pH 5.5) to the neutral pH of plasma during exocytosis [14]. In addition, tubulation and thus WPB elongation influences VWF function as shorter WPBs excrete VWF with a reduced functionality [24]. Besides VWF, WPBs also store angiopoietin-2 (Ang-2), p-selectin, interleukin 8, eotaxin-3, calcitonin gene related peptide, endothelin (EDN1), endothelin converting enzyme (ECE1), CD63, alpha 1,3 fucosyltransferase VI, tissue

type plasminogen activator (tPA), osteoprotegerin, factor VIII and Rab proteins [11,25-27], indicating the importance of functional WPBs as all these molecules are essential for proper endothelial performance [20]. The maturation process of VWF is an important determinant of recruitment and composition of WPB cargo into the TGN [12,28].

Shear stress is a key regulator of VWF gene expression, WPB formation and stimulates ECs to switch from a migratory and proliferative state during angiogenesis (tip- and stalk cells) to a quiescent state (phalanx cells) [27,29]. Physiological shear stress also initiates a vasodilatory, antithrombotic, anti-inflammatory and antioxidant phenotype and therefore is athero-protective [26]. Blood flow induces upregulation of transcription factor Krüppel-like factor 2 (KLF2), which has proven to consistently control the expression of many genes involved in functionally mature endothelium as it acts as a transcriptional switch between the quiescent and activated state [24,30,31]. Another important regulatory environmental cue in formation and stabilization of the vasculature derives from pericytes, mural cells originating from the vascular smooth muscle lineage which line capillary walls [32]. These cells are involved in the regulation of angiogenesis, blood flow, structural stabilisation of the vasculature and vascular permeability[33]. Taken together, stimulation of KLF2 expression and co-culture with pericytes are both involved in the stabilization of vasculature and could provide an instructive environment for hiPSC-ECs maturation.

Here, we explored the effect of environmental stimuli as shear stress, KLF2 overexpression and pericyte co-culture on the VWF and WPB phenotype as a standard for hiPSC-ECs maturity. As shear stress in EC is also a key regulator of glycolysis, we hypothesized that associated changes in cell metabolism in hiPSC-ECs may be a modulator of VWF and WPB maturation.

Materials and methods

Human induced pluripotent stem cell culture and EC differentiation

NCRM1 was obtained from RUCDR Infinite Biologics, Piscataway USA (generated by reprogramming of CD34+ cord blood using episomal vectors). LUMC0072iCTRL01 (L72) and LUMC0099iCTRL04 (L99) were generated by the LUMC iPSC core facility on mouse embryonic fibroblasts (MEFs) using Simplicon RNA Reprogramming Kit (Millipore-Merck, Amsterdam, the Netherlands) and ReproRNA (Stem Cell Technologies, Köln, Germany) respectively, as described previously (Yoshioka et al., 2013) and further cultured in TeSR-E8 medium (Stem Cell Technologies). The hiPSC-ECs were generated from these lines according to Orlova, et al. [3] and after isolation,

hiPSC-ECs were transferred to EC serum- free medium (EC-SFM, Gibco, Thermo-Fisher Scientific, Waltham, USA) (EC-SFM) to which platelet-poor plasma serum (1% vol/vol) (Biomedical Technologies Inc., Stoughton, USA), 50 µg/mL VEGF-165 (R&D Systems, Biomedical Technologies) and 100 µg/mL basic fibroblast growth factor (hFGF) (Miltenyi Biotech, Bergisch Gladbach, Germany), VEGF and basic fibroblast growth factor (bFGF) had been added (EC-SFM full medium) at 37 °C with 5% CO_2. and antibiotics (100 IU/mL penicillin and 100 µg/mL streptomycin) as described in detail before [34]. Results of RNA sequencing were obtained and reproduced in ECs from three different hiPSC lines (hiPSC-L72, hiPSC-L99 and hiPSC-NCRM1). All other results are from NCRM1 (also used as undifferentiated control).

Primary human microvascular EC (hMVECs) culture

hMVECs are isolated from human kidney cortical tissue and were purchased from Cell Systems (ACBRI-128, Kirkland, WA). They were available at Passage 3 (< 12 cumulative population doublings) cryopreserved in CSC Cell Freezing Medium (4Z0-705). hMVECs were also cultured in EC-SFM full medium at 37 °C with 5% CO_2 and antibiotics (100 IU/mL penicillin and 100 µg/mL streptomycin).

Human kidney-derived perivascular stromal cells (hkPSCs) culture

hkPSC were isolated from transplant grade kidneys discarded for as surgical waste [35].FACS confirmed homogeneous NG2 positive hkPSC populations between passages 4-8 and hMVEC between passages 6-8, were cultured in EC-SFM full medium at 37°C and 5% CO_2 as described in detail before [34].

Flow experiments

Shear experiments were performed using an Ibidi flow system (Ibidi, Martinsried, Germany) and described elsewhere [34]. In short, cells were cultured for 4 days at a constant laminar shear stress of 5 dyne/cm^2 in EC-SFM full medium. Cells were seeded into closed perfusion chambers(IbiTreat 0.4 µ-Slide I or VI, Luer) coated with 0.2% porcine gelatin (Sigma-Aldrich) at a concentration of 1.5*106 cells per mL and allowed to adhere for 3 hours. Thereafter, the chamber was connected to a computer-controlled air pressure pump and a fluidic unit with a two-ways switching valve. The pump setup allowed pumping of 16 mL cell culture medium from two reservoirs in a unidirectional way through the flow channel over the monolayer of ECs at a constant shear stress of 5 dyne/cm^2. Medium was refreshed after day 1 of culture. The chamber and the reservoirs containing the medium are kept in an incubator at 37 °C and 5% CO_2. RNA was isolated from cells subjected to shear stress in a 0.4 µ-Slide I Luer flow chamber, while the 6 lanes of a 0.4 µ-Slide VI Luer are used for immunofluorescent staining.

Confocal immunofluorescence microscopy

After exposure to flow or static conditions (at day 4), hMVECs and hiPSC-ECs were fixed in freshly made 4% paraformaldehyde (Alfa Aesar, Thermo Fisher, Haverhill, USA) in HBSS (Invitrogen, Thermo Fisher Scientific, Carslbad, USA) for 10 minutes at room temperature, washed twice with HBSS /1% BSA (Sigma-Aldrich, Saint Louis USA) and then blocked for 30 minutes with 5% BSA in HBSS at room temperature. 0.2% Triton (Sigma-Aldrich) was added during fixation to permeabilize the cells. Cells are incubated overnight (16 hours) at 4 °C with primary antibodies: VWF-Fitch (1ug/mL, ab8822 Abcam, Cambridge, UK), VE-cadherin (1ug/mL, R&D Systems, MAB9381), Ang-2 (1ug/mL, AF623 R&D systems), P-selectin (0.5ug/mL, 556087, BD, Franklin Lakes, USA), Ki-67 (0.5ug/mL, 550609, BD) and the appropriate control IgG1 or IgG2a isotype antibodies (X0931, Dako, Santa Clara, USA ; 559319, BD) diluted in HBSS/1% BSA. After washing three times with HBSS/1% BSA, cells are incubated with Hoechst 33258 (H3569, Life Technologies, Thermo Fisher Scientific) and the appropriate secondary antibody (1:500) goat-α-mouse labeled with Alexa 488/568 (Molecular Probes Eugene, USA, IgG1: A11001, A11004; IgG2a: A21134, A21131) for 2 hours at 4 °C. Cells were again washed for three times with HBSS/1% BSA and covered with dabco glycerol. Cells were imaged using a Leica SP8 white light laser confocal immunofluorescence microscopy.

Sequential 12-bit confocal images (xyz dimensions, 0.142×0.142×0.3µm, 0.142×0.142×1µm or 0.116x0.116×1µm) were recorded using LASX Image software (Leica) and analyzed with ImageJ. VWF was quantified as percentage of positive stained cells, defined as minimal of 1 clear group of pixels of VWF staining within cell, of the total cells per field of view. From each independent experiment (n = 4) 200 cells were analyzed.

Western blotting

After the hMVECs and hiPSC-ECs reached a confluent state, they were lysed in lysis buffer (50mM Tris-HCl, 150 mM NaCl, 1% SDS Deoxycholate,0,5% Triton X-100) supplemented with protease inhibitor (1:100). Sonoporation was used to achieve complete cell disrupture. The protein concentration was determined with a BCA protein kit (Thermo Fisher). Loading samples consisting of Red Pack loading buffer (NEB), SDS-page, lysis buffer supplemented with protease inhibitor and 6,5 µg protein sample were incubated at 95 degrees for 10 minutes. Proteins, transferred on a nitrocellulose membrane (Biorad) were detected with antibodies against VWF (A0082 Dako), MYC (5605S Cell Signalling, Leiden, The Netherlands), MYCN (84406, Cell signalling) MCT1 (20139-1-AP ProteinTech, Manchester, UK) and GAPDH (DIGH11, Cell signalling). After incubation, the membrane was washed and incubated with a HRP-conjugated secondary antibody (p0047, Dako) at room temperature for 1 hour. Afterwards, signal was generated after 5 minutes of incubation in ECL (Perkin Elmer, Waltham, USA) whereupon signal was emitted in a ChemicDoc Imaging System (Biorad, Hercules, USA). The Simple Western™ Wes™ assay of ProteinSimple™ (Bio-Techne) was used to detect MCT1 (1:50, ProteinTech20139-1-AP) and GAPDH (1:20, DIGH11, Cell signalling) according to the manufactorers protocol using 0.2 ug/ul for each sample [36].

RNA isolation and qPCR

After the hMVECs and hiPSC-ECs reached a confluent state (at day 4), they were washed with DPBS whereupon Trizol (Ambion, Thermo Fisher) was added. RNA isolation was achieved using a RNeasy mini kit (Qiagen, Hilden, Germany) and qPCR was performed as previously described[35].Forward and reversed VWF, KLF2 and MCT1 primer sequences are depicted in table 1. Ct values were normalized by the Ct of GAPDH.

VWF primer sequence:	
hu VWF forward	CCGATGCAGCCTTTTCGGA
hu VWF reverse	TCCCCAAGATACACGGAGAGG
KLF2 primer sequence:	
hu KLF2 forward	CTACACCAAGAGTTCGCATCTG
hu KLF2 reverse	CCGTGTGCTTTCGGTAGTG
MCT1 primer sequence:	
hu MCT1 forward	AGTAGTTATGGGAAGAGTCAGCA
hu MCT1 reverse	GTCGGGCTACCATGTCAACA

RNA sequencing

Samples from 3 independent experiments were used for RNA sequencing. For each sample, an indexed cDNA library was prepared from 1µg total RNA using the KAPA stranded mRNA-seq kit (Sopachem, Ochten, The Netherlands). Clusters were generated using the Cbot2 system (Illumina, San Diego, USA) and amplified cDNA fragments were sequenced on a HiSeq 4000 system (Illumina) as follows: 51 cycles for read 1 and 8 cycles for index 1. The raw sequenced reads were mapped to the human reference genome build GRCh38 using STAR [37]. Mapped reads were quantified using RSEM [38] for accurate quantitation resulting in, on average, 34,740,890 ± 8,771,147 counts per sample. After auto-scaling, the resulting data were first summarized by principal component analysis (PCA) using the flashPCA (R package). Plotly was

used to generate interactive graphs (2D plots). Heatmap analysis was performed using the heatmaply package. RNA-sequencing data are available in ArrayExpress (https://www.ebi.ac.uk/arrayexpress/experiments/E-MTAB-8392) under accession E-MTAB-8392.

Lentiviral transductions

The human KLF2 overexpression construct was kindly provided by Prof. A. Horrevoets, VUMC Amsterdam, the Netherlands. Lentiviral particles were produced as described by the Sigma Library protocol using HEK293T cells. For transduction of hMVECs or iPSC-ECs with the lentiviral expression vectors for *KLF2*^{OE} or mock cells were cultured to a 60-80% confluent state in EC-SFM medium and transduced with the respective lentivirus in combination with 8 ug/mL polybrene (Sigma-Aldrich) and incubated for 1 hour (37°C and 5% CO_2). After 1 hour, the transduction medium was replaced with fresh EC-SFM and incubated at 37°C and 5% CO_2, for another 12 hours. Hereafter, the EC-SFM medium was refreshed and the cells were incubated at 37°C and 5% CO_2 for another 12 hours before collecting them for experimental assays.

VWF transfection

For transfection of hiPSC-ECs with VWF plasmid (pcDNA 3.1(+) zeo human VWF-MYC, kindly provided by A. de Jong, LUMC Leiden, The Netherlands[39]), cells were cultured to a 60-80% confluent state in EC-SFM medium and transfected with transfection medium (Cell Applications inc., San Siego, USA, transfection kit) containing transfection medium, CF2 (1:400), PE (1:400) and VWF plasmid (300 ng/mL) for 1 hour at 37°C and 5% CO_2. Hereafter, transfection medium was replaced for fresh EC-SFM and the cells were incubated for 24 hours (37°C, 5% CO_2). Subsequently, the EC-SFM medium was refreshed and after another 24 hours of incubation (37°C, 5% CO_2), the cells were fixed.

Intracellular pH measurements

The cell-permeant pH indicator, carboxy SNARF®-1 acetoxymethyl ester, acetate (Molecular Probe), was used to determine intracellular pH. As described before[40], carboxy-SNARF®-1 exhibits a significant pH-dependent emission shift from yellow-orange to deep red fluorescence under acidic and basic conditions, respectively, enabling the measurement of pH differences between pH 5-9. Cells were plated overnight on a black 96 well plate, then loaded with SNARF-1 for 30 minutes at at 37°C and 5% CO_2. For each cell type, a standard curve of pH's with nigericin (10mM) was taken along. The intracellular pH was determined by the ratio of the fluorescence intensities from the dye at two emission wavelengths - 580 nm and 640 nm – measured by Molecular Devices Spectramax i3x.

Cells were treated with 10mM acetic acid (Merck, Burlington, USA) dissolved in culture medium (pH= 7.1) for 24 hours.

For alkalisation of the intracellular compartments cells were treated with 10µM monensin (R&D systems) in EC-SFM or ECSFM + HCL (pH=7.0) and 10 µM nigericin (Sigma-Aldrich) for 1 hour before fixation.

Proliferation measurement

To determine proliferation activity, ECs were seeded at a density of 20.000 cells in a 24 well plate and left to adhere for 16 hours, followed by 24h treatment with 10mM acetic acid or ECSFM. Subsequently, cells were treated with MTT (5mg/mL, Sigma Aldrich) 1:10 in culture medium and incubated for 2 hours at 37 °C. Afterwards, MTT was removed and isopropanol/0.04M HCL added and measured at 570 nm by Molecular Devices Spectramax i3x. Cellular protein content was determined with a BCA-protein kit from Pierce (Thermo Fischer Scientific) and the data shown as MTT normalized to mg protein.

Analysis of metabolites

Quantitative analysis of intracellular and extracellular metabolites was performed using NMR spectroscopy as described in detail elsewhere [41,42]. Briefly, hMVECs and hiPSC-ECs in triplicates were washed with warm PBS (37°C) to remove the culture medium and quickly quenched with liquid nitrogen to arrest metabolism. The cells well subsequently scraped of the plates and extracted using a cold (-80°C) solution of methanol/chloroform/water, 8.1:0.9:1 (v/v/v). After leaving the samples on dry ice for at least 30 min, the extracts were centrifuged for 20 min at 18000 × g, at -4°C.

Prior to washing cells with PBS, 0.2 mL of culture medium were collected from each sample and mixed with 0.4 mL of cold (-80 °C) 100% LC-grade methanol to extract extracellular metabolites. All samples were subsequently placed at -80°C for at least 30 min and centrifuged for 20 min at 18000 × g, at -4°C.

The supernatants from both cell extracts and culture medium extracts were collected and dried with nitrogen gas. NMR samples of extracts were prepared by dissolving the dried material with 0.22 mL of 0.15 M phosphate buffer (pH 7.4) in deuterated water containing 0.05 mM trimethylsilyl propionic-d_4-sodium salt (TSP-d_4) as internal standard for NMR referencing and quantification. An 1D ^{1}H-NMR spectrum was collected for each sample with a 14.1 T (600 MHz for ^{1}H) Bruker Avance II NMR, using the 1D-NOESY experiment with presaturation as implemented in the spectrometer library (Topspin v3.0, pulse sequence: noesygppr1d; Bruker Biospin, Ltd). All spectra

were processed to correct the phase and baseline and imported in Chenomx NMR suite 8.4 (Chenomx NMR suite, v8.0, Edmonton, Canada) for quantification of metabolites. The protein pellet was dissolved in lysis buffer (150mM NaCl, 1% SDS, 0.5% deoxycholate and 0.5% triton X-100, pH 7.5) with sonification. The protein concentration was measured using PierceTM BCA protein assay kit (ThermoFisher) according to its manual. All concentrations were normalised to the total protein mass of each sample.

For ^{13}C fractional enrichment analysis, two triplicates of hMVEC and hiPSC-ECs were cultured in parallel in either a glucose-free medium, enriched by 5 mM U-$^{13}C_6$-D-Glucose for 24 hours or in medium with non-isotopically enriched D-glucose at the same concentration (5 mM) and processed as described above. Fractional enrichment of ^{13}C-labelled metabolites was calculated using the differences between integrated areas of protons bonded to ^{13}C from those bonded to ^{12}C, as described elsewhere[42].

Uptake or release of metabolites from or to the culture medium, respectively, was calculated as: $((C_{spent} - C_{blank}) \times V)$/ protein, where C_{spent} is the concentration of metabolite in the culure medium (mmol/L), C_{blank} the concentration in the cell-free medium (mmol/L) and V (L) the volume of culture medium in each petri dish. Negative values indicate uptake and positive values indicate release of metabolites.

Statistical analysis

Results are presented as mean ± s.d. or mean ± SEM, n defines the number of biological replicates. Differences between groups were assessed by non-paired 2-tailed Student's t test, paired 2-tailed Student's t test or, when not normally distributed, by two-tailed F-test. Difference between >2 groups was assessed by ANOVA and Tukey's post-hoc testing. P values < 0.05 were considered statistically significant.

Results

hiPSC-derived endothelial cells express an immature endothelial genotype and phenotype

First, we investigated the maturity of hiPSC induced endothelial cells (hiPSC-ECs) compared to control primary human microvascular endothelial cells (hMVECs) and their undifferentiated pre-cursor cells (hiPSCs) by assessing a whole genome RNA expression profile. Principle component analysis demonstrated a distinct clustering of the 3 cell types, indicating different transcriptome profiles (Figure 1a).

Heatmap analysis of endothelial markers revealed increased expression of the early progenitor and stem cell markers *CD34* and *SOX17* in hiPSC-ECs and a reduced VWF gene expression (Figure 1b), indicating an immature EC phenotype. qPCR analysis was performed to confirm VWF mRNA expression of the hiPSC-ECs compared to hMVECs under static conditions (Figure 1c). As demonstrated before, VWF gene expression of hiPSC-ECs is remarkably reduced compared to hMVECs, which is also reflected by lower VWF protein in hiPSC-ECs (Figure 1d, e). We next compared cell morphology of hiPSC-ECs derived from 3 different iPSC lines (NCRM1, L72 and L99) to control for cell line specific effects, to hMVECs under static culture conditions. The hMVECs showed abundancy of elongated WPB's (Figure 1f), where the hiPSC-ECs showed reduced and punctate VWF (Figure 1f). Only ~50% of the hiPSC-ECs were positive for VWF presence (Figure 1g). In addition, the RNA sequencing results of WPB storage components further revealed downregulation of Ras related protein RAB-27A (*RAB27A*) and tissue type plasminogen activator (*PLAT*) in hiPSC-ECs and upregulation of *EDN1* and *ANGPT-2* when compared to hMVECs (Figure 1h). To validate protocol independent immaturity of hiPSC-EC WPB, we compared our results to the accessible RNA-sequencing data of hiPSC-ECs of Wimmer et al[1] and Gu et al[43]. For all genes (Supplemental Figure 1a) and metabolic genes (Supplemental figure 1b) our results (Tiemeier[34]; Orlova et al[3]) cluster with the hiPSC-EC data from Wimmer et al[1], Gu et al[43]. Additionally, the primary ECs used cluster together and differ from the hiPSC-EC. This analysis indicates that independent of the protocol used, differences in primary ECs and hiPSC-EC genotype can be found for each hiPSC-EC differentiation protocol.

Formation of WPB is not induced by shear stress, co-culture or KLF2^{OE}/VWF^{OE}

Prolonged laminar flow upregulates endothelial markers, like FLT1, TEK and NOS3 in hMVECs (Figure 1b). However, VWF gene and protein expression in hiPSC-ECs, is strongly downregulated upon exposure to flow (Figure 2a and b, Supplemental figure 2a). Compared to static conditions flow exposure did not increase VWF and Ang-2 staining in hiPSC-ECs (Figure 2c, Supplemental figure 2a, b) and only 12% of the hiPSC-ECs were positive for the presence of WPBs, significantly lower compared to hMVECs (Figure 2d). Testing the role of human kidney-derived perivascular stromal cells (hkPSCs) in hiPSC-ECs maturation also did not result in formation of WPBs or a notable increase of VWF, which remains as a punctate perinuclear staining in a fraction of cells (Figure 2e). Similarly, about 25% of the hiPSC-ECs in co-culture were positive for VWF presence (Figure 2f). Shear stress, which chronically induces KLF2, directly can affect the production of VWF and, in turn, WPB. Overexpression of KLF2 mRNA (*KLF2*^{OE}) was confirmed by

qPCR, however, this was without effect on VWF gene expression (Supplemental figure 2a). *KLF2*^{OE} resulted in a subtle, but significant increase in VWF protein expression in hiPSC-ECs (Supplemental figure 3b, c). However, confocal imaging of VWF staining revealed that lentiviral *KLF2*^{OE} in hiPSC-ECs did not affect WPB formation in hiPSC-ECs as both mock and hiPSC-ECs *KLF2*^{OE} cells show a similar level of punctate VWF staining (Supplemental figure 3d, e). Finally, VWF transfection was performed to investigate whether WPB immaturity in hiPSC-ECs could be a result of a limited VWF protein presence in these cells. Confocal data showed an increase in VWF staining intensity, however did not improve WPB formation in VWF transfected hiPSC-ECs (Supplemental figure 3f).

VWF tubulation and WPB elongation are dependent on low intracellular pH.

The formation of WPBs is dependent on VWF tubulation by intrachain disulphide bond formation and association of the pro-peptide, after furin cleavage[44], with the mature VWF peptide at the acidic pH of the Golgi, TGN and WPB (Figure 3a)[16,45-50]. Both dimeric bouquets formation and helical arrangement of VWF are pH regulated (Figure 3a)[23,51]. Given the requirement of an acidic intracellular environment for this process, we questioned whether lack of elongated WPBs in hiPSC-ECs could be due to an altered intracellular pH (pHi) regulation. The elongated 'cigar' shape of WPBs in hMVECs (Figure 3b) indeed disappeared after the cells were exposed to nigericin, an antibiotic acting as an antiporter of H+ and K+ and thereby disturbing pHi

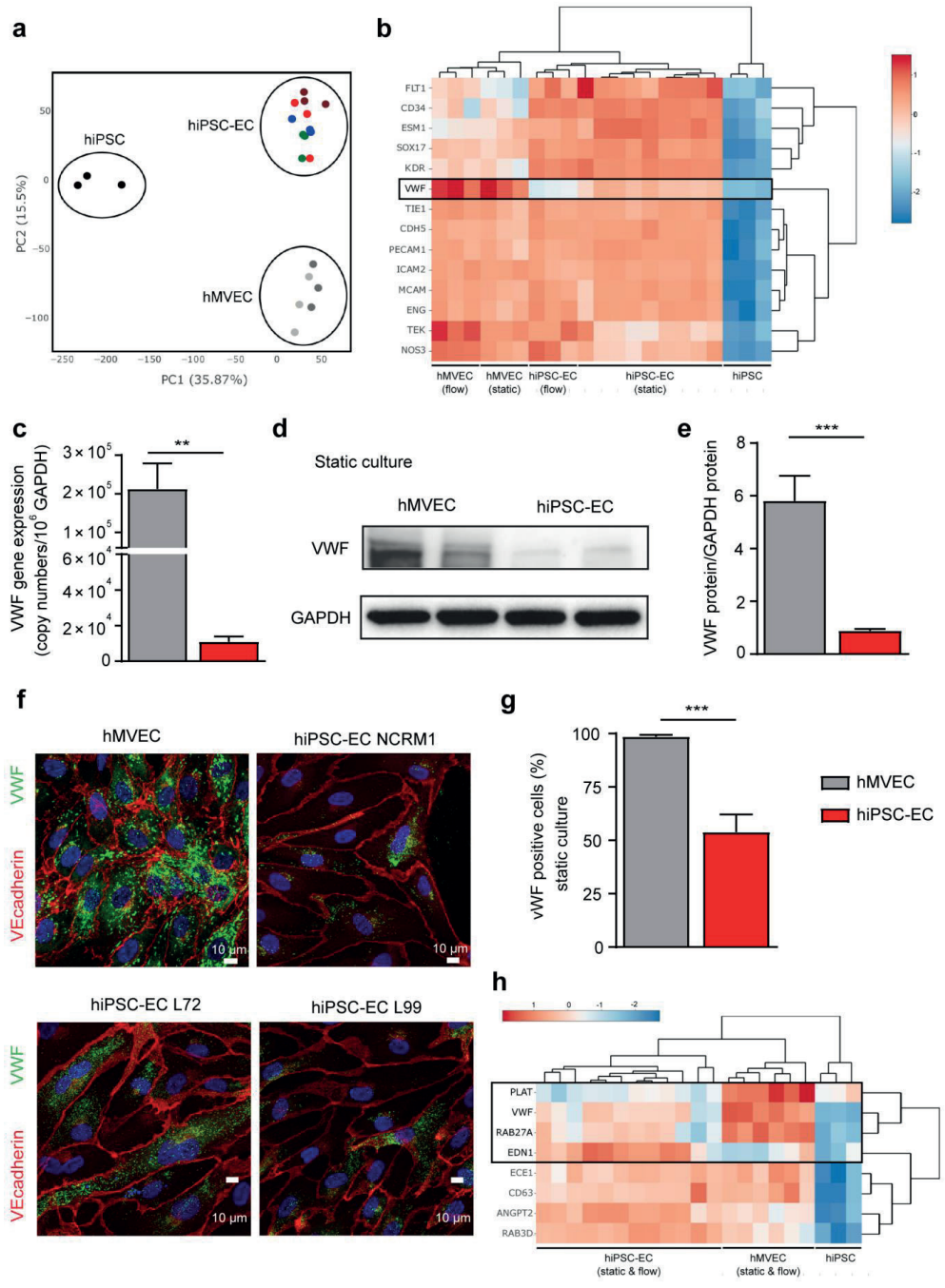

Figure 1. Assessment of hiPSC-ECs maturity.
(a) Principle component analysis of all genes acquired from RNA-sequencing results of hiPSC (black), mature ECs (hMVECs, grey) and hiPSC-ECs in static conditions and after exposure to flow (dark grey: hMVEC and dark red: hiPSC-EC NCRM1). Three hiPSC lines were used to create hiPSC-ECs: NCRM1 (red), L72 (blue), L99 (green). **(b)** Heat map of 14 endothelial markers acquired from RNA-sequencing results of hiPSC, mature ECs (hMVECs) and hiPSC-ECs in static conditions and after exposure to flow. Scale bar represents Z-scores: blue indicates lower gene expression and red, a higher gene expression **(c)** qPCR results of VWF expression of hiPSC-ECs NCRM1 and hMVECs after static culture normalized by GAPDH**. (d)** Western blot analyses of VWF protein expression of hMVECs and hiPSC-ECs NCRM1 after static cell culture. GAPDH was included as a positive control. Blots are representative of three independent experiments. **(e)** Quantification of western blot analyses of VWF protein of hMVECs and hiPSC-ECs NCRM1 after static cell culture. **(f)** Representative cross-sectional confocal images stained for VWF (green) and VE-cadherin (red) after static culture of hMVECs, hiPSC-ECs NCRM1, hiPSC-ECs L72, hiPSC-ECs L99. **(g)** VWF positive cells were quantified (n=200/group). **(h)** Heat map of WPB storage components acquired from RNA-sequencing results of hiPSC, mature ECs (hMVECs) and hiPSC-ECs in static conditions and after exposure to flow. Scale bar represents Z-scores: blue indicates lower gene expression and red, a higher gene expression. Values are given as mean ± SEM of 3-4 independent experiments. Non-paired 2-tailed Student's t-test was performed; *P < 0.05, **P < 0.001, ***P < 0.0001.

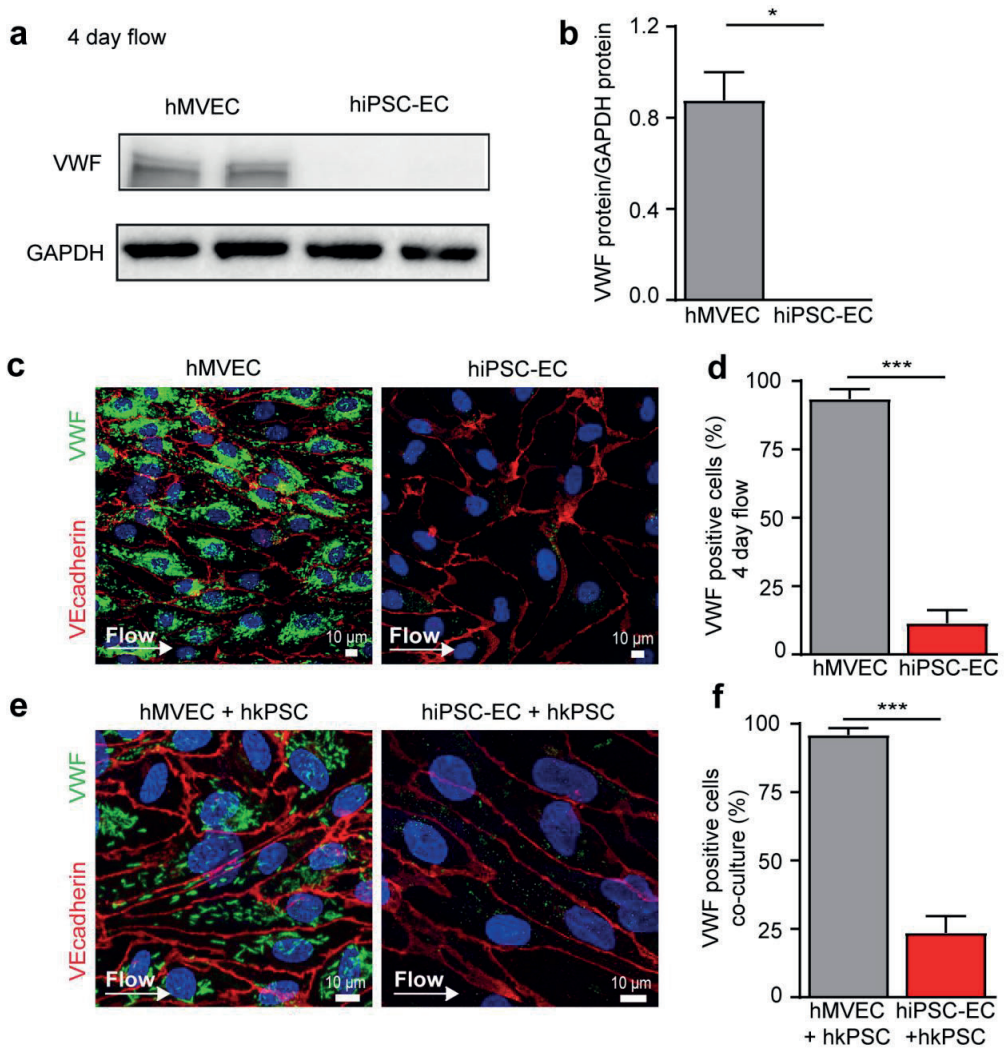

Figure 2. Shear stress and pericyte co-culture do not induce VWF maturation in hiPSC-ECs. **(a)** Western blot analyses of VWF protein expression in hMVECs and hiPSC-ECs NCRM1 after 4 days of laminar flow exposure. Blots are representative of three independent experiments. **(b)** Quantification of western blot analyses of VWF protein of hMVECs and hiPSC-ECs NCRM1 after 4 days of laminar flow exposure. **(c)** Representative cross-sectional confocal images stained for VWF (green) after 4 days of laminar flow of hMVECs and hiPSC-ECs NCRM1. **(d)** VWF positive cells were quantified (n=200/group). **(e)** Representative cross-sectional confocal images stained for VWF (green) after 4 days of laminar flow and co-culture of hMVECs and hiPSC-ECs NCRM1 with hkPSCs. **(f)** VWF positive cells were quantified (n=200/group). Values are given as mean ± SEM of 3-5 independent experiments. Non-paired 2-tailed Student's t-test was performed; *P < 0.05, **P < 0.001, ***P < 0.0001.

maintenance, in medium of pH=7.0 (Figure 3c)[14]. Similar results were obtained after 1 hour appliance of culture medium containing monensin (10 µM), an ionophore that increases pHi by forming lipophilic complexes with monovalent cations to induce Na+ influx and H^+/K^+ efflux, which results in alkalisation of acidic intracellular compartments such as the Golgi apparatus [52] (Figure 3d). These data suggest that an acidic pHi is indeed necessary for VWF tubulation, which in turn drives WPB elongation.

High intracellular pH of hiPSC-ECs impairs WPB formation

The remarkable resemblance of hMVECs WPB phenotype, after increasing the pHi, to the hiPSC-ECs WPBs made us question whether lowering the pHi of the hiPSC-ECs could induce WPB formation in these cells. Addition of monensin, which directly increases pHi, to hiPSC-ECs cell culture medium did not result in a different appearance of the WPBs, indicating that the pHi of hiPSC-ECs was already too high to efficiently form WPBs (Figure 4a). By measuring the pHi with the cell permeable pH indicator SNARF-1, we confirmed that pHi in hiPSC-ECs is higher compared to hMVECs (Figure 4b). To stimulate VWF tubulation in hiPSC-ECs we lowered pHi using 10 mM acetic acid, which was confirmed by pHi measurement (Figure 4b). After lowering the pHi with acetic acid for 24 hours, mature elongated 'cigar' shaped WPBs can be observed in the hiPSC-ECs (Figure 4c) and were positive for VWF, Ang-2 and P-selectin (Supplemental figure 4a and b). This effect on the formation of WPB was independent of the amount of VWF protein, which did not significantly change upon addition of the acid (Supplemental figure 4c, d). Acetic acid addition resulted in an acidification of the culture medium to pH=7.1, causing limited stress to the cells, such as minimal increase in focal adhesion junction, without in Ki-67 expression (Supplemental figure 4e-h). However, hiPSC-EC treated with acetic acid showed a significant increase in proliferation, normalising the proliferation to the level of primary ECs. In hMVEC, addition of acetic acid did not change the proliferation (Supplemental figure 4f).

Low rate of glycolysis could be causal of a high intracellular pH

To understand the mechanism causing an increased pHi and lack of WPB maturation, we performed nuclear magnetic resonance (NMR) analysis to determine the cellular release and uptake of metabolites. hiPSC-ECs were found to have reduced glucose uptake and lactate release, indicating lower glycolysis (Figure 4d and e). This was also reflected in the total intracellular lactate concentration which was significantly lower in hiPSC-ECs as compared to hMVECs (Figure 4f). Carrying out ^{13}C-glucose tracer experiments we determined the intracellular fate of glucose derived metabolites [41,42]. Of the total intracellular lactate, the ^{13}C-lactate fraction was lower in hiPSC-

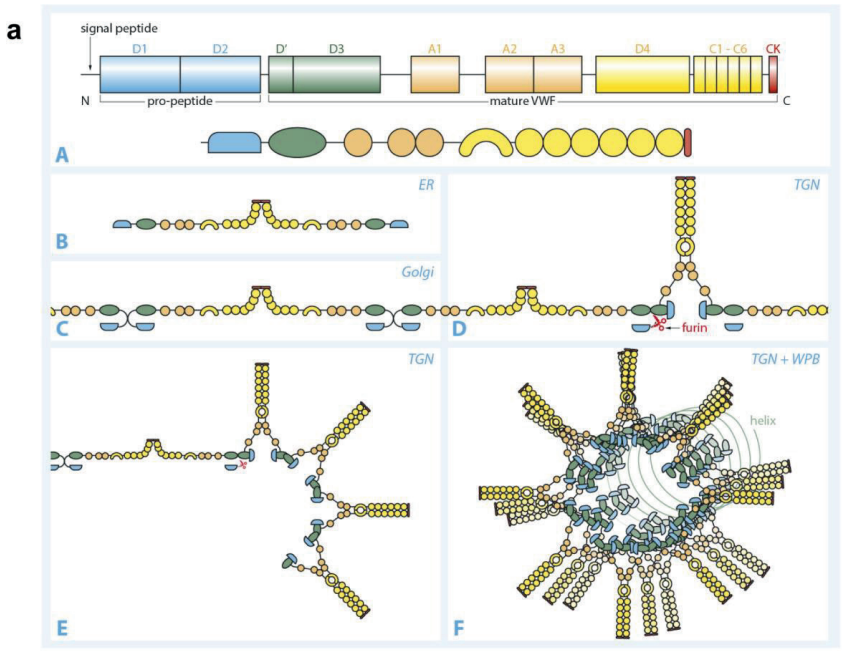

Figure 3. The shape and size of Weibel Palade bodies is pH-dependent. (a) Block diagram showing the domains of pro-peptide (D1-D2), and the regions of the mature protein (D'-CK) involved in dimerization. N, N-terminus; C, C-terminus (panel A). C-terminal dimerization in ER (panel B). N-terminal intrachain disulphide bonds form in the Golgi apparatus (panel C). N-terminal interchain disulphide bonds replace intrachain disulphide bonds and furin cleavage liberates domains D1 and D2 that remain associated with the mature VWF peptide at the acidic pH of the Golgi and WPB (panel D,E). Helical arrangement of the multimeric VWF tubules found in WPB. The N-terminal domains (D1-D2 and D'-D3) form a helix whereas A2-CK fold into a dimeric bouquets, both processes are pH regulated. The sequences neighbouring A1 are likely to function as a flexible hinge allowing the C-terminal part (A2-CK) to pack between adjacent VWF tubules (panel F). Colours of the domains as in panel A.
Representative cross-sectional confocal images stained for VWF (green) (n=3). **(b)** hMVECs cultured in normal medium (EC-SFM). **(c)** hMVECs cultured in pH=7.0 medium (EC-SFM + HCl) containing 10 µM nigericin 1 hour before fixation. **(d)** hMVECs cultured in medium (EC-SFM) containing 10 µM monensin 1 hour before fixation.

ECs (81.6% ± 1.3) compared to hMVECs (90.8% ± 0.7), demonstrating a reduced glycolytic flux towards lactate (Figure 4f). Although oxidative phosphorylation of glucose is at least 20-fold more efficient than glycolysis in producing ATP per mole of glucose, less than 1% of pyruvate is oxidized through the TCA cycle by ECs *in vitro*, while 99% is converted to lactate through glycolysis [53-55]. Both hiPSC-EC and hMVEC were found to convert most glucose into lactate, however hiPSC-EC do this at a significant lower rate (Figure 4d-f). Glycolysis uncoupled from glucose oxidation, resulting in production of $2H^+$ from glycolytically derived ATP hydrolysis [56,57], is a major cause of intracellular acidosis [58]. Taken together, this could partially explain the observed higher pHi in hiPSC-ECs (Figure 4b).

Dysregulation of glycolysis not caused by disturbed MYC and MYCN expression

The regulation of glycolysis in (stem) cell development is regulated by the balance between MYC and MYCN activity. Elevated glycolysis as observed in hiPSCs requires elevated MYC and MYCN activity [59]. Metabolic switching during mesodermal differentiation coincides with a reduction in MYC and MYCN [59]. Since endothelial cells also mainly rely on glycolysis, MYC expression has to be switched on again, which was indeed observed in hiPSC-ECs at a similar level as in hMVECs (Figure 4g), eliminating this balance in expression as a cause for the reduced glycolysis.

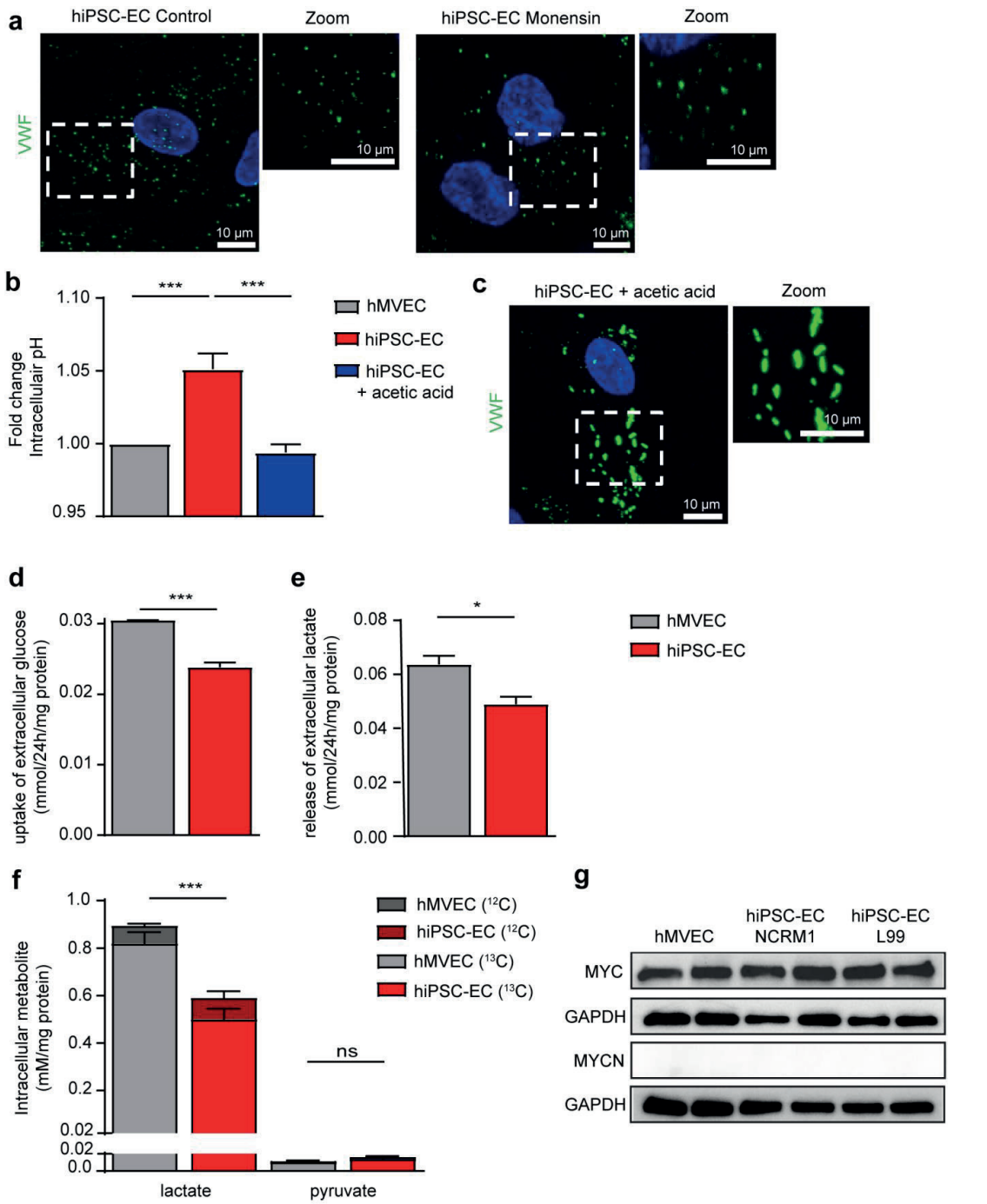

Figure 4. High intracellular pH of hiPSC-EC, caused by low glycolysis, limits WPB formation (a) Representative cross-sectional confocal images stained for VWF (green) of hiPSC-ECs NCRM1 under normal conditions and after 1 hour incubation with 10 µM monensin (n=3). **(b)** Intracellular pH (pHi) of hiPSC-ECs NCRM1 and hMVECs under normal conditions and after 24 hour incubation with acetic acid (10 mM) (n=6). **(c)** Representative cross-sectional confocal images stained for VWF (green) hiPSC-ECs NCRM1 cultured in acetic acid (10 mM) containing medium. **(d)** Glucose uptake rate and **(e)** lactate release rate after 24hrs culture. **(f)** Total intracellular concentrations of lactate and pyruvate and their ^{13}C-enriched fractions after incubation of cells in $^{13}C_6$-D-Glucose containing culture medium for 24h. **(g)** Western blot analyses of MYC and MYCN protein expression in hMVECs, hiPSC-ECs NCRM1 and hiPSC-ECs L99. GAPDH was included as a positive control.
Values are given as mean ± SEM of 3-6 independent experiments. One-way ANOVA and non-paired 2-tailed Student's t-test were performed; *P < 0.05, **P < 0.001, ***P < 0.0001, ns = non-significant.

pHi sensitive lactate/H+ transporter MCT1 downregulated in hiPSC-EC

Intracellular lactate and H+ concentration is not only determined by glycolytic flux but also by the monocarboxylate transporter MCT1, which serves as the main gate for lactate/H^+ entry in endothelial cells [60 61]. In addition to the reduced glycolysis as a cause for low intracellular lactate/H+, we also observed a ~50% downregulation of MCT1 gene expression in hiPSC-ECs (Figure 5a). These results were confirmed at the protein level (Figure 5b and c). MCT1 is known to be directly regulated by pHi, however the alkalic pHi of iPSC-EC does not cause sufficient induction of MCT1 to regulate H+ influx [62]. To verify the involvement of the MCT1 downregulation in disturbed tubulation of VWF, we downregulated MCT1 in hMVECs by transduction with a short hairpin MCT1 construct (shMCT1). This resulted in a ~60% decrease in MCT1 gene expression (Figure 5d) and protein (Figure 5e, f), comparable to the downregulation in hiPSC-ECs. Confocal microscopy revealed similar tubulation problems of the WPBs as increased round and irregular shaped WPBs can be observed in *shMCT1*-hMVECs compared to hMVECs mock (Figure 5g).

To conclude, the formation of mature WPB in hiPSC-ECs is limited by increased intracellular pH (pHi) caused by metabolic dysfunction, such as reduced glycolysis and limited expression of the lactate/H+ transporter MCT1 (Figure 6).

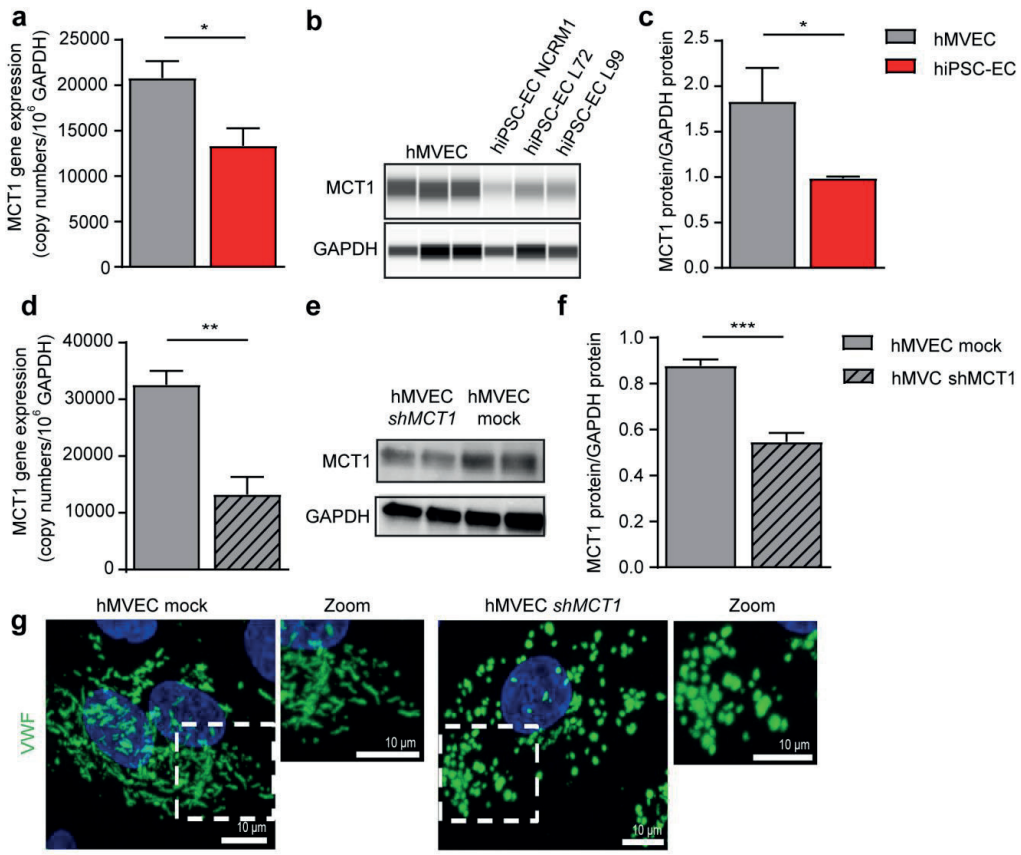

Figure 5. MCT1, a lactate/proton transporter, is involved in WBP maturation. (a) qPCR results of MCT1 expression of hiPSC-ECs NCRM1 and hMVECs. **(b)** SimpleWestern™ Wes™ analysis of MCT1 protein expression in hMVECs and hiPSC-ECs NCRM1, L72 and L99. GAPDH was included as a positive control. Blots are representative of three independent experiments. **(c)** Quantification of Wes™ analysis of MCT1 protein expression in hMVECs and hiPSC-ECs NCRM1, L72 and L99. GAPDH was included as a positive control. **(d)** qPCR results of MCT1 expression of hMVECs mock and lentiviral MCT1 transduced cells. **(e)** qPCR results of MCT1 expression of hMVECs mock and lentiviral MCT1 transduced cells. **(b)** Western blot analyses of MCT1 protein expression in hMVECs mock and after MCT1 transduction. GAPDH was included as a positive control. Blots are representative of three independent experiments. **(c)** Quantification of western blot analyses of MCT1 protein expression in hMVECs mock and MCT2 transduced cells. GAPDH was included as a positive control. **(d)** Representative cross-sectional confocal images stained for VWF (green) of hMVECs mock and lentiviral MCT1 transduced cells. Values are given as mean ± SEM of 3-4 independent experiments. Non-paired 2-tailed Student's t-test were performed; *P < 0.05, **P < 0.001, ***P < 0.0001.

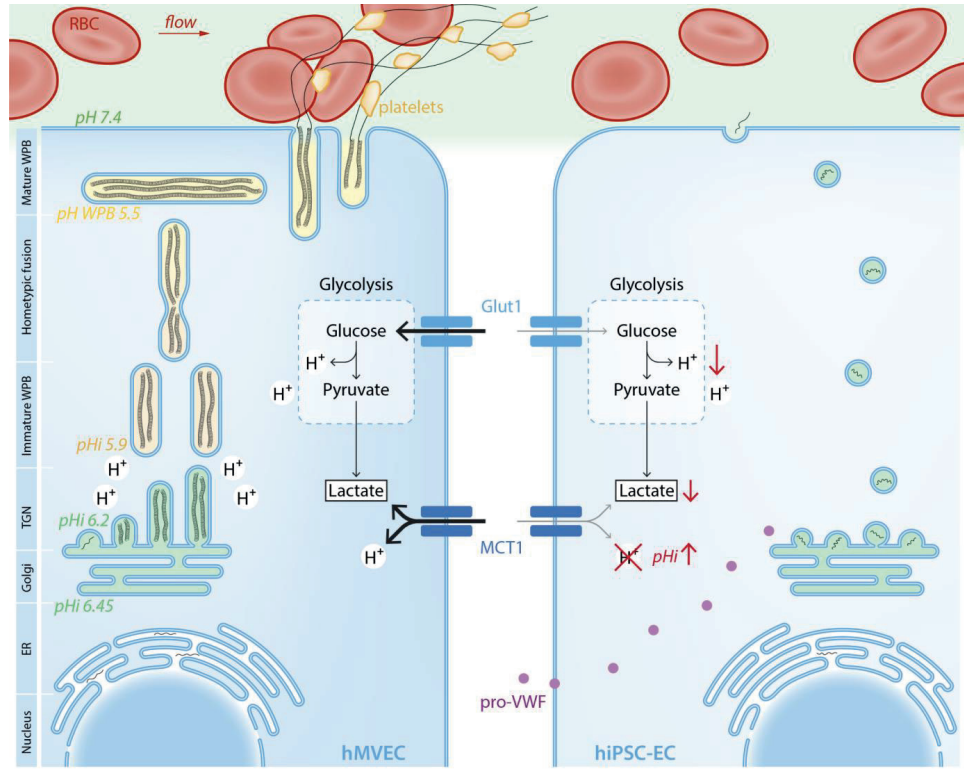

Figure 6. Schematic overview of WPB production and the metabolic regulation of pHi of hMVECs and hiPSC-ECs. Formation of mature WBP in hiPSC-ECs is limited by the increased intracellular pH around the Golgi apparatus and Trans Golgi Network (TGN). This increase in pHi is caused by reduced intracellular lactate accompanied by reduced H^+, caused by reduced glycolysis and reduced uptake of lactate and H^+ via MCT1. This increased pHi limits intrachain disulphide bonds formation and association of the pro-peptide, after furin cleavage, with the mature VWF peptide at the trans-Golgi network (TGN) and WPB. Both dimeric bouquets formation and helical arrangement of VWF are pH regulated. Eventually this reduces the amount of WPB and limits the functionality of the endothelial cell.

Discussion

Here we show that formation of mature WPB in hiPSC-ECs is limited by increased intracellular pH (pHi) around the Golgi apparatus and TGN. This increase in pHi is caused by reduced intracellular lactate accompanied by reduced H^+, as a result of reduced glycolytic flux and reduced cellular uptake of lactate and H^+ via the MCT1 transporter (Figure 6). The resulting increased pHi is known to limit intra chain disulphide bonds formation and association of the pro-peptide, after furin cleavage [44], with the mature

VWF peptide at the TGN and WPB [16,45-50]. Both dimeric bouquets formation and helical arrangement of VWF are pH regulated [23,51]. The hiPSC-ECs WPB maturation can be rescued by acetic acid supplementation, which directly lowered pHi.

Given the critical role of endothelial cells in angiocrine signalling [63], and oxygen and energy transport, the generation of functional hiPSC-derived endothelial cells is a crucial step in the field of stem cell-based disease modelling and regenerative medicine. The current study shows that hiPSC-derived endothelial cells express an immature endothelial geno- and phenotype, which does not improve after exposure to shear stress or KLF2 overexpression. Our data point to a critical role for persisting altered cell metabolism and downstream effects on intracellular pH as the main culprit for WPB maturation failure. Indeed, pluripotent stem cell fate decisions are made through regulation of metabolic flux, where a high rate of anaerobic glycolysis confers stemness [59]. To allow for specification into mesodermal lineages, such as endothelial cells, glycolysis is switched to oxidative phosphorylation through reduction of MYC and MYCN activity. Interestingly, by contrast, mature endothelial cells are characterized by a high glycolytic flux [64]. Our data suggest that this latter adaptation does not fully develop in the EC differentiation protocol, despite increased MYC expression necessary for enhanced glycolysis after MYC and MYCN downregulation during mesoderm differentiation.

Another factor that may have contributed to WPB maturation failure is the observed downregulation of the monocarboxylate transporter member 1 (MCT-1) in hiPSC-ECs. MCTs 1-4 are known to facilitate transmembrane proton cotransport of monocarboxylates such as lactate, pyruvate, acetoacetate and β-hydroxybutyrate across the cell membrane [65]. Since MCT1 is responsible for the import of lactate and H^{+}[49], downregulation of MCT1 in hiPSC-ECs could explain the lower uptake and intracellular concentration of both protons (pHi) and lactate. Lactate is involved in multiple regulatory functions of the cell, including transcriptional stimulation of MCT1, thus coupling reduced glycolytic flux to MCT1 downregulation [65,66].

Generally, the amount of structural and enzymatic components will determine the size or number of organelles[67]. For WPBs, it is well established that the cargo protein VWF is the driver for WPB formation [22]. Gradual reduction in VWF cellular content by siRNA correlated with a gradual decrease in the number of WPBs and, more importantly, also shortening of WPB length [68, 69]. hiPSC-ECs were found to have very low gene expression of VWF and limited amount of VWF protein. Exposing hiPSC-ECs to shear stress did not result in VWF upregulation, probably caused by the reduced glycocalyx surface coat and consequently impaired shear sensing of hiPSC-ECs [34].

Recent work on hiPSC-ECs in 3D models showed improved maturation of hiPSC-ECs and differentiation in to various types of ECs (venular, capillary, arteriolar, arterial) upon transplantation in mice, however VWF expression of these ECs in both 2D and 3D models remained surprisingly low[1].

While direct upregulation of VWF by VWF^{OE} or KLF^{OE} resulted in a slight increase in VWF protein in hiPSC-ECs, WPBs were still limited and round. This underlines the involvement of a post-transcriptional modification problem caused by the metabolic immaturity of hiPSC-ECs. Although we demonstrated that decreasing the pHi in hiPSC-ECs induced WPB maturation without an increase in VWF gene expression, the low amount of VWF protein potentially plays a role in the WPB formation. Assessment of combinatory effects of both VWF^{OE} to induce VWF production and addition of acidic acid to restore WBP formation would be of further interest to optimize the function of WPBs in hiPSC-ECs.

Apart from VWF, several other proteins that regulate endothelial function can be recruited to the WPBs [11,18,25-27,47]. The composition of the WPB is essential to EC organotypic function; e.g. in lung ECs, WPB contain factor VIII clotting factor. The exact composition also determines processes such as vessel stability, where Ang-2 derived from WPBs may dysregulate pericyte stabilization of ECs and induce angiogenesis [70,71].

Conclusion

Although differentiation of hiPSCs into endothelial-like cells (hiPSC-ECs) has been demonstrated before, hiPSC-EC fail to express mature WPBs. Maturation of WPB is a key requirement to generate functional EC from iPSC, as WPB are essential for angiogenesis, primary and secondary homeostasis. Our data show that such WPB maturation failure can be rescued in cell culture by lowering the increased pHi by adding acetic acid. Along the same lines one can speculate about similar strategies that reduce pH or increase glycolytic flux in ECs in organoid cultures to achieve tissue maturation [72].

Acknowledgements

We acknowledge the support of Manon Zuurmond and Loes Wiersma (LUMC, Leiden, the Netherlands). We thank hiPSC core facility (LUMC) for providing two hiPSC lines (LUMC0072iCTRL01 and LUMC0099iCTRL04) and Christine Mummery (LUMC) for providing hiPSC line NCRM1.

This work is supported by the partners of 'Regenerative Medicine Crossing Borders' (RegMed XB) and Powered by Health~Holland, Top Sector Life Sciences & Health.

GLT is funded by the LUMC MD/PhD track and CWvdB is supported by the Wiyadharma fellowship (Bontius Stichting, LUMC).

Author contributions

G.L.T., R.dK. and B.M.vdB: concept and design, collection/assembly of data, data analysis and interpretation, manuscript writing. G.W., S.D., R.G.J.R. and S.K.: collection/assembly of data, data analysis and interpretation. W.M.P.J.S.: collection of data. C.vdB., M.G. and J.C.J.E.: read the manuscript and provided helpful comments. P.C.: Financial support, read the manuscript and provided helpful comments. T.J.R.: concept and design, manuscript writing and financial support.

Conflict of interest

"The authors have declared that no conflict of interest exists."

References

1. Wimmer RA, Leopoldi A, Aichinger M, et al. Human blood vessel organoids as a model of diabetic vasculopathy. *Nature.* 2019;565(7740):505-510.
2. Ong SB, Lee WH, Shao NY, et al. Calpain Inhibition Restores Autophagy and Prevents Mitochondrial Fragmentation in a Human iPSC Model of Diabetic Endotheliopathy. *Stem cell reports.* 2019;12(3):597-610.
3. Orlova VV, van den Hil FE, Petrus-Reurer S, Drabsch Y, Ten Dijke P, Mummery CL. Generation, expansion and functional analysis of endothelial cells and pericytes derived from human pluripotent stem cells. *Nature protocols.* 2014;9(6):1514-1531.
4. Rufaihah AJ, Huang NF, Jame S, et al. Endothelial cells derived from human iPSCS increase capillary density and improve perfusion in a mouse model of peripheral arterial disease. *Arteriosclerosis, thrombosis, and vascular biology.* 2011;31(11):e72-79.
5. Rufaihah AJ, Huang NF, Kim J, et al. Human induced pluripotent stem cell-derived endothelial cells exhibit functional heterogeneity. *American journal of translational research.* 2013;5(1):21-35.
6. Li Z, Hu S, Ghosh Z, Han Z, Wu JC. Functional characterization and expression profiling of human induced pluripotent stem cell- and embryonic stem cell-derived endothelial cells. *Stem cells and development.* 2011;20(10):1701-1710.
7. Park SW, Jun Koh Y, Jeon J, et al. Efficient differentiation of human pluripotent stem cells into functional CD34+ progenitor cells by combined modulation of the MEK/ERK and BMP4 signaling pathways. *Blood.* 2010;116(25):5762-5772.
8. Halaidych OV, Freund C, van den Hil F, et al. Inflammatory Responses and Barrier Function of Endothelial Cells Derived from Human Induced Pluripotent Stem Cells. *Stem cell reports.* 2018;10(5):1642-1656.
9. Adams WJ, Zhang Y, Cloutier J, et al. Functional vascular endothelium derived from human induced pluripotent stem cells. *Stem cell reports.* 2013;1(2):105-113.
10. Deanfield John E, Halcox Julian P, Rabelink Ton J. Endothelial Function and Dysfunction. *Circulation.* 2007;115(10):1285-1295.
11. Nightingale T, Cutler D. The secretion of von Willebrand factor from endothelial cells; an increasingly complicated story. *Journal of thrombosis and haemostasis : JTH.* 2013;11 Suppl 1:192-201.
12. Valentijn KM, Sadler JE, Valentijn JA, Voorberg J, Eikenboom J. Functional architecture of Weibel-Palade bodies. *Blood.* 2011;117(19):5033-5043.
13. Leebeek FW, Eikenboom JC. Von Willebrand's Disease. *The New England journal of medicine.* 2016;375(21):2067-2080.
14. Michaux G, Abbitt KB, Collinson LM, Haberichter SL, Norman KE, Cutler DF. The physiological function of von Willebrand's factor depends on its tubular storage in endothelial Weibel-Palade bodies. *Developmental cell.* 2006;10(2):223-232.
15. Lenting PJ, Christophe OD, Denis CV. von Willebrand factor biosynthesis, secretion, and clearance: connecting the far ends. *Blood.* 2015;125(13):2019-2028.
16. Springer TA. von Willebrand factor, Jedi knight of the bloodstream. *Blood.* 2014;124(9):1412-1425.
17. Sadler JE. Biochemistry and genetics of von Willebrand factor. *Annual review of biochemistry.* 1998;67:395-424.
18. Wang JW, Valentijn KM, de Boer HC, et al. Intracellular storage and regulated secretion of von Willebrand factor in quantitative von Willebrand disease. *The Journal of biological chemistry.* 2011;286(27):24180-24188.
19. Randi AM, Laffan MA. Von Willebrand factor and angiogenesis: basic and applied issues. *Journal of thrombosis and haemostasis : JTH.* 2017;15(1):13-20.
20. Metcalf DJ, Nightingale TD, Zenner HL, Lui-Roberts WW, Cutler DF. Formation and function of Weibel-Palade bodies. *Journal of cell science.* 2008;121(Pt 1):19-27.

21. J. V, R. F, J. C, H. J, J.A. M, H. P. Biogenesis of von Willebrand factor-containing organelles in heterologous transfected CV-1 cells. *The EMBO Journal.* 1993;12(2):749-758.
22. Wagner DD, Saffaripour S, Bonfanti R, et al. Induction of specific storage organelles by von Willebrand factor propolypeptide. *Cell.* 1991;64(2):403-413.
23. Zhou Y-F, Eng ET, Nishida N, Lu C, Walz T, Springer TA. A pH-regulated dimeric bouquet in the structure of von Willebrand factor. *The EMBO Journal.* 2011;30(19):4098-4111.
24. Doddaballapur A, Michalik Katharina M, Manavski Y, et al. Laminar Shear Stress Inhibits Endothelial Cell Metabolism via KLF2-Mediated Repression of PFKFB3. *Arteriosclerosis, thrombosis, and vascular biology.* 2015;35(1):137-145.
25. Rondaij MG, Bierings R, Kragt A, van Mourik JA, Voorberg J. Dynamics and plasticity of Weibel-Palade bodies in endothelial cells. *Arteriosclerosis, thrombosis, and vascular biology.* 2006;26(5):1002-1007.
26. Chistiakov DA, Orekhov AN, Bobryshev YV. Effects of shear stress on endothelial cells: go with the flow. *Acta physiologica (Oxford, England).* 2017;219(2):382-408.
27. Potente M, Gerhardt H, Carmeliet P. Basic and therapeutic aspects of angiogenesis. *Cell.* 2011;146(6):873-887.
28. Harrison-Lavoie KJ, Michaux G, Hewlett L, et al. P-Selectin and CD63 Use Different Mechanisms for Delivery to Weibel–Palade Bodies. *Traffic.* 2006;7(6):647-662.
29. Doddaballapur A, Michalik KM, Manavski Y, et al. Laminar shear stress inhibits endothelial cell metabolism via KLF2-mediated repression of PFKFB3. *Arteriosclerosis, thrombosis, and vascular biology.* 2015;35(1):137-145.
30. Dekker RJ, Boon RA, Rondaij MG, et al. KLF2 provokes a gene expression pattern that establishes functional quiescent differentiation of the endothelium. *Blood.* 2006;107(11):4354-4363.
31. Wang G, Kostidis S, Tiemeier GL, et al. Shear Stress Regulation of Endothelial Glycocalyx Structure Is Determined by Glucobiosynthesis. *Arteriosclerosis, thrombosis, and vascular biology.* 2019:Atvbaha119313399.
32. Enge M, Bjarnegard M, Gerhardt H, et al. Endothelium-specific platelet-derived growth factor-B ablation mimics diabetic retinopathy. *Embo j.* 2002;21(16):4307-4316.
33. Ferland-McCollough D, Slater S, Richard J, Reni C, Mangialardi G. Pericytes, an overlooked player in vascular pathobiology. *Pharmacology & therapeutics.* 2017;171:30-42.
34. Gesa L. Tiemeier GW, Sébastien J. Dumas, Wendy M.P.J. Sol, M. Cristina Avramut, Tobias Karakach, Valeria V. Orlova, Cathelijne W. van den Berg, Christine L. Mummery, Peter Carmeliet, Bernard M. van den Berg, Ton J. Rabelink. Closing the Mitochondrial Permeability Transition Pore in hiPSC-Derived Endothelial Cells Induces Glyococalyx Formation and Functional Maturation. *Stem cell reports.* 2019;Vol.1 13:1-14.
35. Leuning DG, Reinders ME, Li J, et al. Clinical-Grade Isolated Human Kidney Perivascular Stromal Cells as an Organotypic Cell Source for Kidney Regenerative Medicine. *Stem cells translational medicine.* 2017;6(2):405-418.
36. Nguyen U, Squaglia N, Boge A, Fung PA. The Simple Western™: a gel-free, blot-free, hands-free Western blotting reinvention. *Nature methods.* 2011;8:982.
37. Dobin A, Davis CA, Schlesinger F, et al. STAR: ultrafast universal RNA-seq aligner. *Bioinformatics (Oxford, England).* 2013;29(1):15-21.
38. Li B, Dewey CN. RSEM: accurate transcript quantification from RNA-Seq data with or without a reference genome. *BMC bioinformatics.* 2011;12:323.
39. de Jong A, Dirven RJ, Oud JA, Tio D, van Vlijmen BJM, Eikenboom J. Correction of a dominant-negative von Willebrand factor multimerization defect by small interfering RNA-mediated allele-specific inhibition of mutant von Willebrand factor. *Journal of Thrombosis and Haemostasis.* 2018;16(7):1357-1368.
40. van Borren MM, den Ruijter HM, Baartscheer A, Ravesloot JH, Coronel R, Verkerk AO. Dietary Omega-3 Polyunsaturated Fatty Acids Suppress NHE-1 Upregulation in a Rabbit Model of Volume- and Pressure-Overload. *Frontiers in physiology.* 2012;3:76.
41. Kostidis S, Addie RD, Morreau H, Mayboroda OA, Giera M. Quantitative NMR analysis of intra- and extracellular metabolism of mammalian cells: A tutorial. *Analytica Chimica Acta.* 2017;980:1-24.

42. Vinaixa M, Rodríguez MA, Aivio S, et al. Positional Enrichment by Proton Analysis (PEPA): A One-Dimensional 1H-NMR Approach for 13C Stable Isotope Tracer Studies in Metabolomics. *Angewandte Chemie International Edition.* 2017;56(13):3531-3535.
43. Gu M, Shao NY, Sa S, et al. Patient-Specific iPSC-Derived Endothelial Cells Uncover Pathways that Protect against Pulmonary Hypertension in BMPR2 Mutation Carriers. *Cell stem cell.* 2017;20(4):490-504.e495.
44. Feliciangeli SF, Thomas L, Scott GK, et al. Identification of a pH sensor in the furin propeptide that regulates enzyme activation. *The Journal of biological chemistry.* 2006;281(23):16108-16116.
45. Wagner DD, Mayadas T, Marder VJ. Initial glycosylation and acidic pH in the Golgi apparatus are required for multimerization of von Willebrand factor. *The Journal of cell biology.* 1986;102(4):1320-1324.
46. Llopis J, McCaffery JM, Miyawaki A, Farquhar MG, Tsien RY. Measurement of cytosolic, mitochondrial, and Golgi pH in single living cells with green fluorescent proteins. *Proceedings of the National Academy of Sciences of the United States of America.* 1998;95(12):6803-6808.
47. Metcalf DJ, Nightingale TD, Zenner HL, Lui-Roberts WW, Cutler DF. Formation and function of Weibel-Palade bodies. *Journal of cell science.* 2008;121(1):19-27.
48. Michaux G, Abbitt KB, Collinson LM, Haberichter SL, Norman KE, Cutler DF. The Physiological Function of von Willebrand's Factor Depends on Its Tubular Storage in Endothelial Weibel-Palade Bodies. *Developmental cell.* 2006;10(2):223-232.
49. Casey JR, Grinstein S, Orlowski J. Sensors and regulators of intracellular pH. *Nature reviews Molecular cell biology.* 2010;11(1):50-61.
50. Crimi E, Taccone FS, Infante T, Scolletta S, Crudele V, Napoli C. Effects of intracellular acidosis on endothelial function: an overview. *Journal of critical care.* 2012;27(2):108-118.
51. Gerke V. Von Willebrand factor folds into a bouquet. *The EMBO journal.* 2011;30(19):3880-3881.
52. Mollenhauer HH, Morre DJ, Rowe LD. Alteration of intracellular traffic by monensin; mechanism, specificity and relationship to toxicity. *Biochimica et biophysica acta.* 1990;1031(2):225-246.
53. De Bock K, Georgiadou M, Schoors S, et al. Role of PFKFB3-driven glycolysis in vessel sprouting. *Cell.* 2013;154(3):651-663.
54. Eelen G, de Zeeuw P, Treps L, Harjes U, Wong BW, Carmeliet P. Endothelial Cell Metabolism. *Physiological reviews.* 2018;98(1):3-58.
55. Krutzfeldt A, Spahr R, Mertens S, Siegmund B, Piper HM. Metabolism of exogenous substrates by coronary endothelial cells in culture. *Journal of molecular and cellular cardiology.* 1990;22(12):1393-1404.
56. Delvin TM. *Textbook of Biochemistry with clinical correlations.* Vol 6th edition: Wiley-Liss.; 2006.
57. Jeremy M. Berg JLT, Lubert Tryer, Gregory J Gatto Jr. *Biochemistry.* Vol 7th edition: W.H. Freeman and Company; 2012.
58. Dyck JR, Lopaschuk GD. Glucose metabolism, H+ production and Na+/H+-exchanger mRNA levels in ischemic hearts from diabetic rats. *Molecular and cellular biochemistry.* 1998;180(1-2):85-93.
59. Cliff TS, Wu T, Boward BR, et al. MYC Controls Human Pluripotent Stem Cell Fate Decisions through Regulation of Metabolic Flux. *Cell stem cell.* 2017;21(4):502-516.e509.
60. Sonveaux P, Copetti T, De Saedeleer CJ, et al. Targeting the lactate transporter MCT1 in endothelial cells inhibits lactate-induced HIF-1 activation and tumor angiogenesis. *PLoS One.* 2012;7(3):e33418.
61. Halestrap AP, Wilson MC. The monocarboxylate transporter family--role and regulation. *IUBMB life.* 2012;64(2):109-119.
62. Uhernik AL, Tucker C, Smith JP. Control of MCT1 function in cerebrovascular endothelial cells by intracellular pH. *Brain Research.* 2011;1376:10-22.

63. Rafii S, Butler JM, Ding B-S. Angiocrine functions of organ-specific endothelial cells. *Nature.* 2016;529(7586):316-325.
64. Eelen G, de Zeeuw P, Treps L, Harjes U, Wong BW, Carmeliet P. Endothelial Cell Metabolism. *Physiological reviews.* 2018;98(1):3-58.
65. Sun S, Li H, Chen J, Qian Q. Lactic Acid: No Longer an Inert and End-Product of Glycolysis. *Physiology (Bethesda, Md).* 2017;32(6):453-463.
66. Hui S, Ghergurovich JM, Morscher RJ, et al. Glucose feeds the TCA cycle via circulating lactate. *Nature.* 2017;551:115.
67. Goehring NW, Hyman AA. Organelle growth control through limiting pools of cytoplasmic components. *Current biology : CB.* 2012;22(9):R330-339.
68. Ferraro F, Kriston-Vizi J, Metcalf Daniel J, et al. A Two-Tier Golgi-Based Control of Organelle Size Underpins the Functional Plasticity of Endothelial Cells. *Developmental cell.* 2014;29(3):292-304.
69. McCormack JJ, Harrison-Lavoie K, Cutler DF. Human endothelial cells size-select their secretory granules for exocytosis to modulate their functional output. *Journal of thrombosis and haemostasis : JTH.* 2019.
70. Maisonpierre PC, Suri C, Jones PF, et al. Angiopoietin-2, a natural antagonist for Tie2 that disrupts in vivo angiogenesis. *Science (New York, NY).* 1997;277(5322):55-60.
71. Zhang L, Yang N, Park JW, et al. Tumor-derived vascular endothelial growth factor up-regulates angiopoietin-2 in host endothelium and destabilizes host vasculature, supporting angiogenesis in ovarian cancer. *Cancer research.* 2003;63(12):3403-3412.
72. van den Berg CW, Ritsma L, Avramut MC, et al. Renal Subcapsular Transplantation of PSC-Derived Kidney Organoids Induces Neo-vasculogenesis and Significant Glomerular and Tubular Maturation In Vivo. *Stem cell reports.* 2018;10(3):751-765.

Supplementary Figures

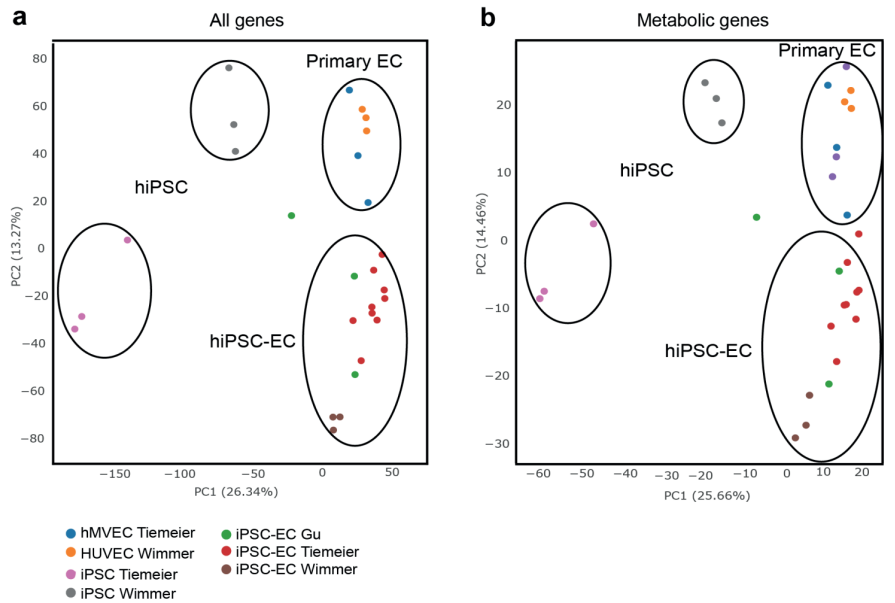

Supplementary figure 1. Comparison of hiPSC-EC differentiation protocols by RNA-sequencing. Principle component analysis of all genes **(a)** and metabolic genes **(b)** acquired from RNA-sequencing results of hiPSC (Wimmer et al: pink , Tiemeier et al: grey), primary mature ECs (HUVEC: orange, hMVECs: blue) and hiPSC-ECs derived by several differentiation protocols (Wimmer et al: brown, Gu et al: green, Tiemeier et al: red) in static 2D conditions. Tiemeier et al. used three hiPSC lines to create hiPSC-ECs: NCRM1, L72, L99.

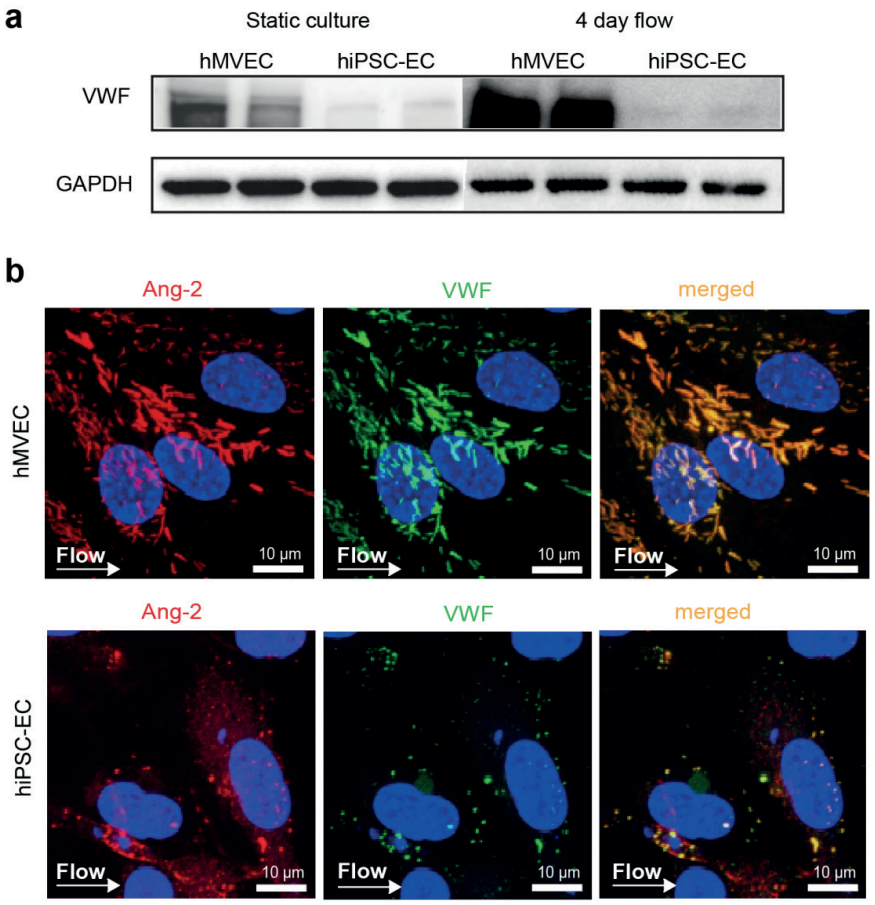

Supplementary figure 2. Lack of Weibel Palade Bodies in hiPSC-ECs. (a) Western blot analyses of VWF protein expression of hMVECs and hiPSC-ECs NCRM1 after static cell culture and after 4 days laminar flow. GAPDH was included as a positive control. Blots are representative of three independent experiments. **(b)** Representative cross-sectional confocal images stained for VWF (green) and Ang-2 (red) of hMVECs and hiPSC-ECs NCRM1.

Supplementary figure 3. hiPSC-ECs WPB phenotype of KLF2 transduced cells. (a) qPCR results of KLF2 and VWF expression in hMVECs and hiPSC-ECs NCRM1 mock and lentiviral KLF2 transduced cells (*KLF2*^{OE}). **(b)** Western blot analyses of VWF protein expression in hMVECs and hiPSC-ECs NCRM1 mock and after KLF2 transduction. GAPDH was included as a positive control. Blots are representative of three independent experiments. **(c)** Quantification of western blot analyses of VWF protein expression in hMVECs and hiPSC-ECs NCRM1 mock and *KLF2*^{OE} of hMVECs and hiPSC-ECs NCRM1. GAPDH was included as a positive control. **(d)** Representative cross-sectional confocal images stained for VWF (green) of hMVECs mock and *KLF2*^{OE}. **(e)** Representative cross-sectional confocal images stained for VWF (green) of hiPSC-ECs NCRM1 mock and *KLF2*^{OE}. **(g)** Representative cross-sectional confocal images stained for VWF (green) and MYC-plasmid (red) of hiPSC-ECs NCRM1 after VWF transfection (*VWF*^{OE}). Values are given as mean ± SEM of 3 independent experiments. One-way ANOVA was performed; *P < 0.05, **P < 0.001, ***P < 0.0001.

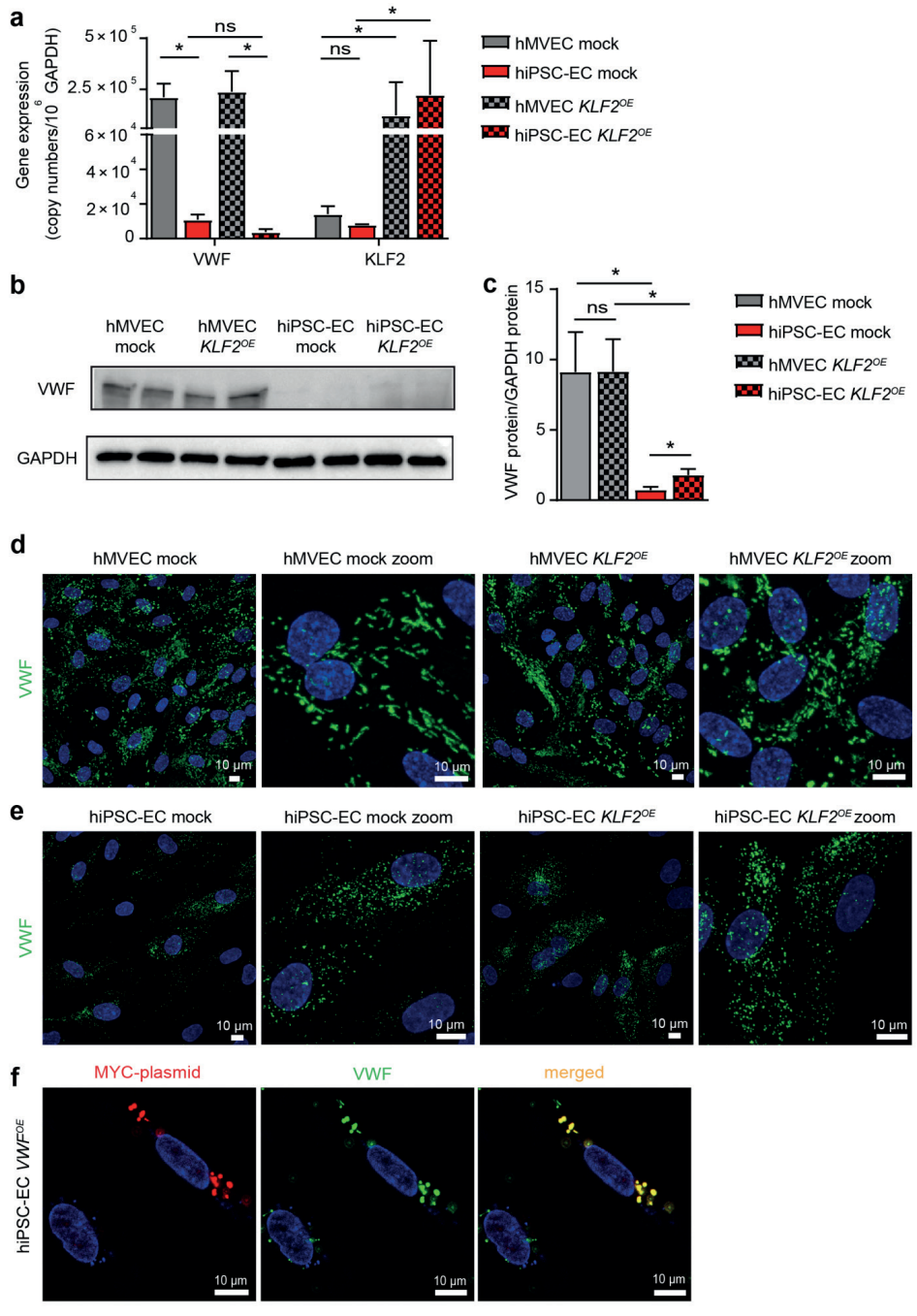

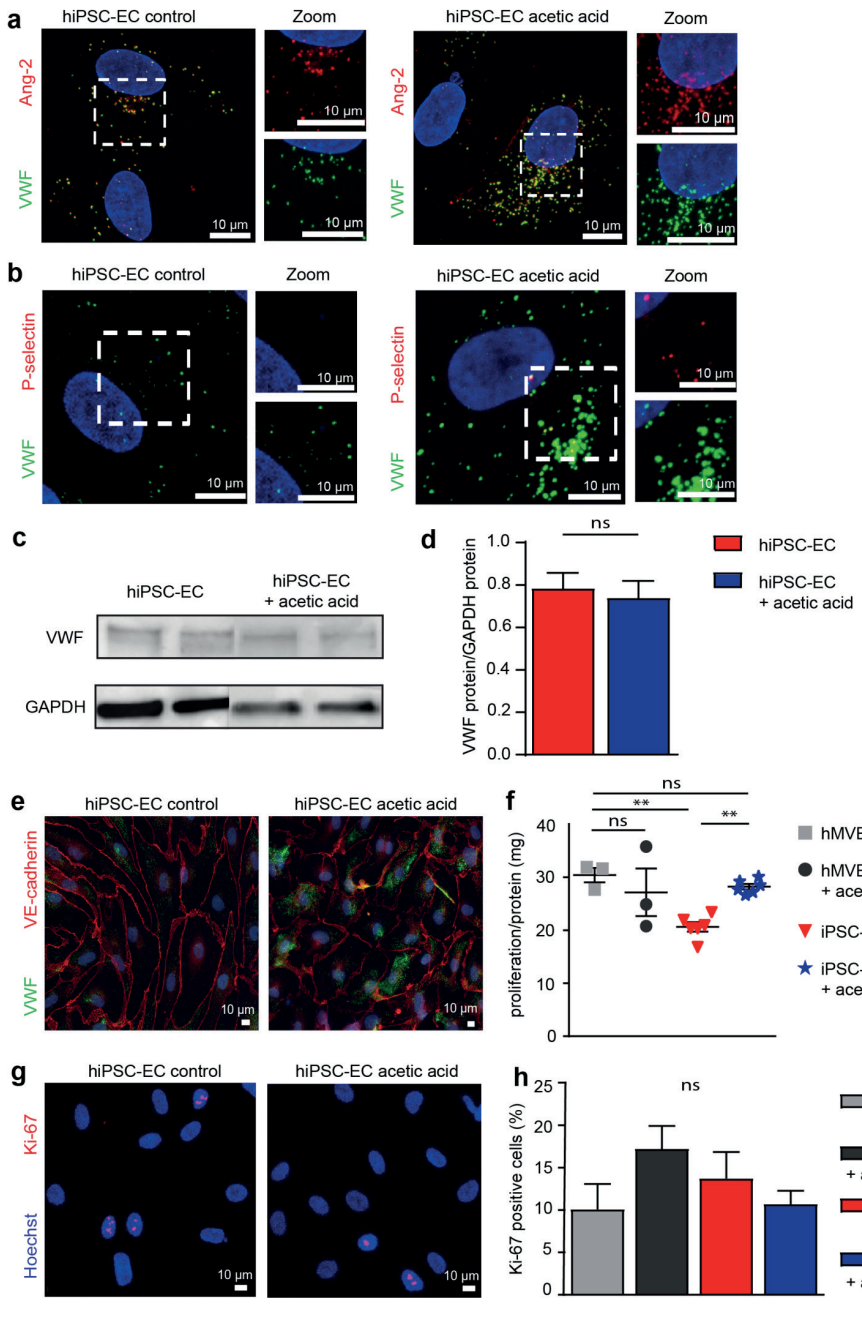

Supplementary figure 4. Effects of acetic acid addition in hiPSC-ECs. **(a)** Representative cross-sectional confocal images of iPSC-ECs stained for Ang-2 (red), VWF (green) and Hoechst (blue) after 24h of culture with 10mM acetic acid. **(b)** Representative cross-sectional confocal images of iPSC-ECs stained for P-selectin (red), VWF (green) and Hoechst (blue) after 24h of culture with 10mM acetic acid. **(c)** Western blot analyses of VWF protein expression in hiPSC-ECs NCRM1 control and after culturing in acetate acid (10 mM) containing medium. GAPDH was included as a positive control. Both taken from same blot. Blots are representative of three independent experiments. **(d)** Quantification of western blot analyses of VWF protein expression in hiPSC-ECs NCRM1 control and of hiPSC-ECs NCRM1 cultured in acetate acid (10 mM) containing medium. GAPDH was included as a positive control. **(e)** Representative cross-sectional confocal images of iPSC-ECs stained for VE-cadherin (red), VWF (green) and Hoechst (blue) after 24h of culture with 10mM acetic acid. **(f)** Proliferation rate of hMVEC and hiPSC-ECs measured by MTT assay normalized by mg protein after 24h culture with 10mM of acetic acid. **(g)** Representative cross-sectional confocal images of iPSC-ECs stained for ki-67 (red) and Hoechst (blue) after 24h of culture with 10mM acetic acid. **(h)** Quantification of ki-67 positive cells (n=200-500). Values are given as mean ± SEM of 3 independent experiments. Non-paired 2-tailed Student's t-test or One-Way ANOVA were performed; *P < 0.05, **P < 0.001, ***P < 0.0001, ns = non-significant.